Radical Salt-Doped Hole Transporters in Organic Photovoltaic Devices

SanthiSagar Vaddiraju,[†] Mathew Mathai,[†] Emmanuel Kymakis,[‡] and Fotios Papadimitrakopoulos*[,†,§]

Nanomaterials Optoelectronics Laboratory, Polymer Program, Institute of Materials Science, and Department of Chemistry, University of Connecticut, Storrs, Connecticut 06269-3136, and Electrical Engineering Department, Technological Educational Institute (T.E.I.) of Crete, Estavromenos P.B. 1939, Heraklion, GR-71 004 Crete, Greece

Received March 16, 2007. Revised Manuscript Received June 2, 2007

Efficient photovoltaic devices were demonstrated from thick polymer films (2500 Å), using ternary mixtures of C_{60}, a polycarbonate linked TPD (*N*,*N*,*N*′,*N*′-tetrakis(phenyl)benzidine)) polymer (PTPD), and a small molecular weight radical salt of a TPD derivative, in an indium tin oxide/blend/Al configuration. The binary PTPD mixtures with salt and C_{60} were also investigated in a similar device configuration. The addition of the radical salt increases the hole conductivity of the PTPD host matrix and subsequently enhances the photocurrent by 1 order of magnitude. On the other hand, blending PTPD with C_{60} increases the photocurrent by 3 orders of magnitude to produce a short circuit current (I_{sc}) of 0.22 mA/cm^2. The incorporation of these two binary systems into a ternary blend shows a further increase in the I_{sc} (0.33 mA/cm^2) with a power conversion efficiency of 0.47%. To the best of our knowledge this is the first time that a radical salt has been used in an organic photovoltaic device configuration. This study provides insight on the interplay of the three components of this ternary system to both open circuit voltage (V_{oc}) and I_{sc}. Further optimization in structure and morphology of these devices can lead to significant performance enhancement.

Introduction

The unique photophysical and semiconducting properties of conjugated organic systems along with the relative ease in device fabrication have generated significant interest for uses in organic light emitting diodes, photovoltaic devices, and memory devices.[1,2] Photovoltaic devices that can be fabricated by inkjet printing and reel to reel lamination processes provide revolutionary approaches to decrease cost and increase production efficiency.[3,4] At present, manufacturing controlled architectures with precise film thicknesses at the submicrometer range presents a major challenge to the above-mentioned fabrication methodologies.[5−7] This challenge has in part been resolved in the case of xerography, where thick layers (≥ 1 μm) of hole transporting materials routinely coat the drums of every copy-making machine.[8] Such thick hole transporting layers typically comprise a polymeric binder doped with radical salts of small molecular weight (MW) hole transporters.[6] In particular, radical salts of triphenylamine, tri-*p*-tolylamine, hydrazones, and pyrazolines blended with polycarbonates and polystyrene present one of the favored xerographic hole transporting systems.[9−12] In this study we present our initial findings in using such systems in organic photovoltaic configuration in an attempt to increase film thickness and potentially alleviate some of the required tolerances associated with the films.

While thicker films are beneficial for complete light absorption, the low exciton diffusion length of typical π-conjugated polymers presents a major problem.[13] This problem is in part alleviated by the creation of multiple heterojunctions from microphase separation of hole and electron transporting materials.[14−16] The optimum device thickness is determined by the balance of the light-generated field, the carrier mobilities of holes and electrons, and the

* To whom correspondence should be addressed. Tel.: +1 860 486 3447. Fax: +1 860 486 4745. E-mail address: papadim@mail.ims.uconn.edu.

† Nanomaterials Optoelectronics Laboratory, Polymer Program, Institute of Materials Science, University of Connecticut.

‡ Technological Educational Institute.

§ Department of Chemistry, University of Connecticut.

(1) Friend, R. H. *Pure Appl. Chem.* **2001**, *73*, 425.
(2) Kelley, T. W.; Baude, P. F.; Gerlach, C.; Ender, D. E.; Muyres, D.; Haase, M. A.; Vogel, D. E.; Theiss, S. D. *Chem. Mater.* **2004**, *16*, 4413.
(3) Brabec, C. J.; Hauch, J. A.; Schilinsky, P.; Waldauf, C. *MRS Bull.* **2005**, *30*, 50.
(4) Brabec, C. J. *Sol. Energy Mater. Sol. Cells* **2004**, *83*, 273.
(5) Pardo, D. A.; Jabbour, G. E.; Peyghambarian, N. *Adv. Mater.* **2000**, *12*, 1249.
(6) Abkowitz, M. A. *Synth. Met.* **2004**, *141*, 29.
(7) Shaheen, S. E.; Radspinner, R.; Peyghambarian, N.; Jabbour, G. E. *Appl. Phys. Lett.* **2001**, *79*, 2996.
(8) Borsenberger, P. M.; Weiss, D. S. *Organic Photoreceptors for Xerography*; Dekker: New York, 1998.
(9) Khan, F.; Hor, A.-M.; Sundararajan, P. R. *Pure Appl. Chem.* **2004**, *76*, 1509.
(10) Borsenberger, P. M.; Magin, E. H.; Sinicropi, J. A.; Lin, L.-B. *Jpn. J. Appl. Phys.* **1998**, *37*, 166.
(11) Tameev, A. R.; Hea, Z.; Milburn, G. H. W.; Kozlov, A. A.; Vannikov, A. V.; Puchala, A.; Rasala, D. *Appl. Phys. Lett.* **2002**, *81*, 969.
(12) Khan, F.; Hor, A.-M.; Sundararajan, P. R. *Synth. Met.* **2005**, *150*, 199.
(13) Nelson, J. *Curr. Opin. Solid State Mater. Sci.* **2002**, *6*, 87.
(14) Coakley, K. M.; McGehee, M. D. *Appl. Phys. Lett.* **2003**, *83*, 3380.
(15) Greenham, N. C.; Peng, X.; Alivisatos, A. P. *Phys. Rev. B: Condens. Matter* **1996**, *54*, 17628.
(16) Yu, G.; Gao, J.; Hummelen, J. C.; Wudl, F.; Heeger, A. J. *Science* **1995**, *270*, 1789.

10.1021/cm070744c CCC: $37.00
Published on Web 07/17/2007

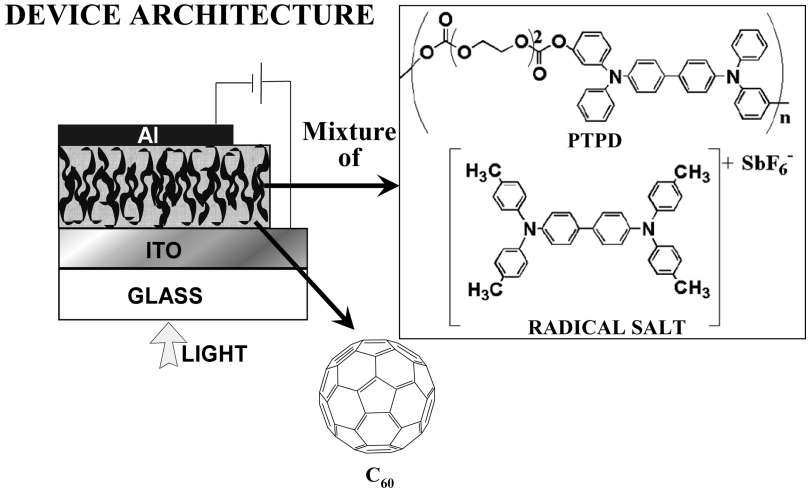

Figure 1. Device configuration of the fabricated photovoltaic cells along with the chemical structures of the compounds used in this study.

extinction coefficient of the photoactive components.[17] The degree of crystallinity in both hole and electron transporting phases generally exerts enormous influence to carrier mobilities. Unlike small MW organics (i.e., C_{60} and its derivative like [6,6]-phenyl-C61 butyric acid methyl ester (PCBM)) that crystallize more readily in confined geometries, polymeric hole transporters crystallize with greater difficulty in similar architectures. In addition, in bulk heterojunction devices, the crystallinity of the high MW component is often restricted by the presence of a low MW *n*-type component, further decreasing hole mobility. On the basis of these arguments, thick polymer/C_{60} or PCBM bulk heterojunction devices should experience greater drop in hole rather than electron mobility. Polymer regioregularity and annealing are crucial for improving crystallinity and hole mobility; however, the internal field generated by light is typically low to overcome the proportionally greater number of traps as device thicknesses increase above 1000 Å.[18−22]

The xerographic approach, which generally employs thick (>1 μM), amorphous semiconducting films, could potentially be employed to mitigate the aforementioned problem with hole mobility. The hole transporting layer used in xerography is typically composed of a thick glassy solid "solution" of a low MW organic semiconductor dispersed in a polymeric binder. Such coatings are typically cast from solution common to both of the components.[6] More conductive films employ a three component blend of a charge transport molecule, an oxidized charge transport molecule, and a polymer binder.[23] The oxidized charge transport moiety is a radical salt, where controlled oxidation renders this low MW organic in its polaronic state.[23] Typically such oxidized organic salt dopant has the same chemical functionality as that of the host material and thus provides a way by which hole doping can be uniformly distributed throughout the film.[23] These amorphous systems have been extensively studied for their charge transport and mobility and are known to be providing relatively high mobility at large thicknesses.[23−25]

Figure 1 illustrates the structure of a hole transporting polycarbonate polymer (PTPD) composed of alternative *N*,*N*′-bis(3-hydroxymethyl)-*N*,*N*′-bis(phenyl)benzidine and diethylene glycol units.[26−29] In the same figure, the structure of the $TMPTD^{\bullet+}$ SbF_6^- organic radical salt is shown, produced by the reaction of *N*,*N*,*N*′,*N*′-tetrakis(4-methylphenyl)benzidine (TMTPD) with $HSbF_6$.[23] When such salt is introduced to 5000 Å thick PTPD films, their conductivity is increased by 2−3 orders of magnitude.[23] This system has been successfully used as thick hole transporting layers in OLED devices and was also shown to minimize the indium tin oxide (ITO)/hole transport layer junction resistance.[30] The salt to polymer ratio was also shown to behave as a tunable resistor for hole transport.[30]

In this paper we demonstrate the application of this radical salt doped polymer in organic solar cells, as a thick (2500 Å) photoactive layer in conjunction with C_{60}. X-ray diffraction (XRD) revealed the totally amorphous nature of PTPD in both the presence and the absence of the radical salt. Apart from the advantages gained from using thicker amorphous photoactive films (which leads to increased absorption of the incident light), the hole conductivity of these thicker films can be readily increased by increasing the concentration of the salt.[23,25] This favorable role of salt is directly reflected in the performance of PTPD/salt binary system devices wherein the I_{sc} increased by an order of magnitude due to

(17) Brabec, C. J. *Sol. Energy Mater. Sol. Cells* **2004**, *83*, 273.
(18) Hoppe, H.; Arnold, N.; Meissner, D.; Sariciftci, N. S. *Thin Solid Films* **2004**, *451*−*452*, 589.
(19) Duren, J. K. J. v.; Yang, X.; Loos, J.; Bulle-Lieuwma, C. W. T.; Sieval, A. B.; Hummelen, J. C.; Janssen, R. A. J. *Adv. Funct. Mater.* **2004**, *14*, 425.
(20) Li, G.; Shrotriya, V.; Huang, J.; Yao, Y.; Moriarty, T.; Emery, K.; Yang, Y. *Nat. Mater.* **2005**, *4*, 864.
(21) Liu, J.; Shi, Y.; Yang, Y. *Adv. Funct. Mater.* **2001**, *11*, 420.
(22) Shaheen, S. E.; Brabec, C. J.; Sariciftci, N. S.; Padinger, F.; Fromherz, T.; Hummelen, J. C. *Appl. Phys. Lett.* **2001**, *78*, 841.
(23) Hsieh, B. R. *Polym. Prepr. (Am. Chem. Soc., Div. Polym. Chem)* **2002**, *43*, 452.
(24) Pope, M.; Swenberg, C. E. *Electronic Processes in Organic Crystals and Polymers*; Oxford University Press: Oxford, 1999.
(25) Shen, Y.; Diest, K.; Wong, M. H.; Hsieh, B. R.; Dunlap, D. H.; Malliaras, G. G. *Phys. Rev. B: Condens. Matter* **2003**, *68*, 081204-1.
(26) Hsieh, B. R. U.S. Patent 5,853,906, 1998.
(27) Hsieh, B. R.; Ewing, J. R.; VanLaeken, A. C. U.S. Patent 5,968,674, 1999.
(28) Mort, J.; Hsieh, B. R.; Machonkin, M. A.; Mammino, J. U.S. Patent 5,834,080, 1998.
(29) Yanus, J. F.; Spiewak, J. W.; Renfer, D. S.; Limburg, W. W. U.S. Patent 5,028,687, 1991.
(30) Mathai, M. K.; Papadimitrakopoulos, F.; Hsieh, B. R. *J. Appl. Phys.* **2004**, *95*, 8240.

the presence of salt. Incorporation of the radical salt into the PTPD/C_{60} mixture provided seven times improvement, from 0.06% to 0.47% in the power conversion efficiency (η_E). Barring the recent report on the use of amorphous liquid-phase tris[4-(2-methoxyethoxy)phenyl]amine (mixed with a *p*-dopant and a redox inactive ionic dopant) in dye sensitized "Grätzel" type solar cells,[31] to the best of our knowledge this is the first study on the application of radical salt doped amorphous polymers in organic photovoltaic devices.

Experimental Section

The PTPD polymer and the radical salt of the TPD derivative were received as a gift from Dr. Bing Hsieh and used as is.[30] Buckminster fullerene (C_{60}) was purchased from Aldrich and used as received.

XRD data were collected on a Bruker GADDS instrument. The PTPD polymer sample (with no salt) was in the form of a pellet positioned at the end of a fine capillary tube. The background was subtracted by running a blank experiment on the glass capillary itself. In the case of PTPD/salt binary blend with 10% (w/w) loading, a film was cast from a methylene chloride solution, lifted off the glass substrate with the help of water, rolled, and inserted in a fine glass capillary tube prior to XRD analysis. Similar procedure was utilized for the XRD analysis of PTPD/salt/C_{60} ternary blends, where *o*-dichlorobenzene was used as solvent instead of methylene chloride.

UV−vis absorption spectra were obtained from films cast on quartz substrates using the aforementioned solvents. The data was collected on a Perkin-Elmer Lambda 6 spectrophotometer, and the background was subtracted by running a blank sample of plain quartz substrate.

Cyclic voltammetry (CV) experiments were employed to determine the oxidation and reduction potential of the various compounds used in this study. These measurements were performed on a CH Instruments (Model 840B) potentiostat outfitted with Pt working and counter electrodes while the reference electrode was Ag/AgCl. A 0.1 M solution of tetraethyl ammonium tetrafluoroborate (TEATFB) in dimethyl formamide (DMF) was used as an electrolyte for the CV. All the solutions were purged with nitrogen before measurement. The sweep rate was 50 mV/s, and the concentration of the electroactive species was approximately 0.2 mg/mL. The Ag/AgCl reference electrode was calibrated with respect to the ferrocene standard (~4.8 eV), and the corresponding highest occupied molecular orbital (HOMO) and lowest unoccupied molecular orbital (LUMO) levels of the electroactive compounds were calculated using their CV-obtained $E_{1/2}^{\mathrm{Red}}$ and $E_{1/2}^{\mathrm{Ox}}$ values using the following empirical relation:

$$E^{\mathrm{HOMO/LUMO}} = [-e(E_{\mathrm{onset(vsAg/AgCl)}} - E_{\mathrm{onset(Fe/Fe^{+}vsAg/AgCl)}})] - X \text{ eV}$$

where X is the ferrocene value of 4.8 eV.[32]

Photovoltaic devices were fabricated on ITO coated glass slides (8−12 Ω/□) procured from Aldrich. Diodes were fabricated in a sandwich configuration, as shown in Figure 1, by spin coating the photoactive films on top of a cleaned pre-patterned ITO substrates.[30] The thickness of the active layer was around 2500 Å. Following spin coating in air, aluminum (Al) electrodes (approximately 500 Å) were thermally evaporated at vacuum greater than 4×10^{-6} Torr. After fabrication, all devices were transferred to a nitrogen filled glovebox without exposure to oxygen or moisture (using a load lock cell) for characterization and testing. Current density−voltage ($J-V$) measurements were obtained on a Hewlett-Packard 4155A semiconductor parameter analyzer. A SoLux solar lamp (intensity of 15 mW/cm^2) was used to illuminate the sample. Forward bias is defined as positive voltage applied to the ITO electrode.

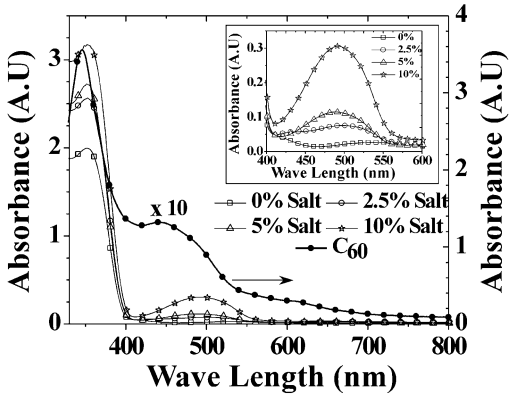

Figure 2. UV−vis of the PTPD film (open symbols, left ordinate) spin-coated from a methylene chloride solution on a quartz substrate. The concentration of radical salt in the polymer was varied to be 0%, 2.5%, 5%, and 10% with respect to the PTPD polymer. Also shown is the absorbance of an evaporated C_{60} film on quartz substrate (closed circles, right ordinate). (Top Inset) The absorbance of the radical salt in the 400−600 nm range alone.

Binary (PTPD/salt) and tertiary (PTPD/salt/C_{60}) films were fabricated by spin coating from a 15 mg/mL solution in *o*-dichlorobenzene, to produce uniform films of approximately 2500 Å. While both PTPD and salt are readily miscible in *o*-dichlorobenzene, sonication was utilized to solubilize C_{60} in the same solvent, followed by filtration through a 0.45 μm PTFE filter to remove particulates. Two sets of ternary blend devices were prepared: (T1) devices have C_{60} concentration fixed at 50 wt % with respect to the PTPD, while the salt amount is varied from 0 to 10 wt % with respect to PTPD. (T2) devices have the PTPD to salt ratio fixed at either 0 or 10%, while the C_{60} loading varied from 0 to 50% with respect to PTPD. The T2 devices with 0% and 10% salt are termed as T2A and T2B devices, respectively.

Results and Discussion

UV−Vis Absorption Spectra of PTPD/Salt Binary Mixtures. Figure 2 illustrates the UV−vis absorption spectra of 5000 Å spin-coated films on quartz of PTPD and PTPD/TMTPD$^{\bullet+}$SbF$_6^-$ radical salt binary blends with varying salt concentrations. The primary absorption of PTPD is centered 352 nm while that of TMTPD$^{\bullet+}$SbF$_6^-$ salt is centered around 490 nm and increases progressively with increasing concentration as shown in the inset of Figure 2. The UV−vis absorption of an evaporated C_{60} thin film (20 nm) is also shown for comparison with two broad absorptions in 345 and 450 nm. The long tail past the 450 nm absorption peak is due to crystallization induced scattering.

Energy Levels of PTPD and TMTPD$^{\bullet+}$SbF$_6^-$ Radical Salt. The cyclic voltammograms (CV) of PTPD and TMTPD$^{\bullet+}$ SbF$_6^-$ radical salt in DMF are shown in Figure 3. The voltammogram of PTPD exhibits single oxidation and reduction peaks with onset corresponding to 0.35 and −2.75 V with respect to Ag/AgCl reference electrode, respectively.

(31) Snaith, H. J.; Zakeeruddin, S. M.; Wang, Q.; Péchy, P. t.; Gratzel, M. *Nano Lett.* **2006**, *6*, 2000.
(32) Al-Ibrahim, M.; Roth, H. K.; Zhokhavets, U.; Gobsch, G.; Sensfuss, S. *Sol. Energy Mater. Sol. Cells* **2005**, *85*, 13.

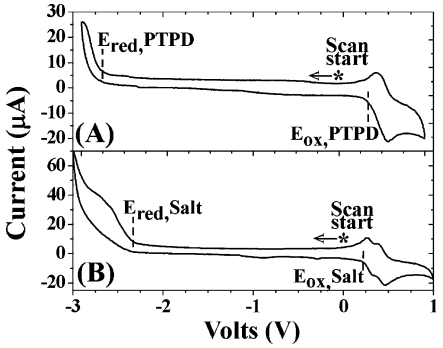

Figure 3. Cyclic voltammograms of PTPD (A) and $TMTPD^{\bullet+}$ SbF_6^- radical salt (B) obtained in a three electrode cell consisting of platinum working and counter electrodes and an Ag/AgCl reference electrode in 0.1 M solution of TEATFB in DMF.

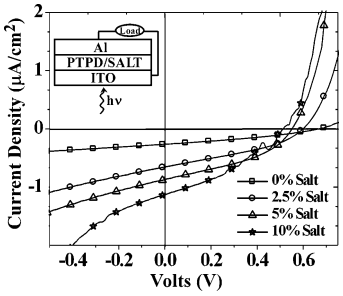

Figure 4. *J*−*V* characteristics under illumination of the ITO/PTPD−salt/Al binary blend devices with varying salt concentrations. The inset shows the device configuration used.

These values correspond to 5.15 and 2.05 eV with respect to vacuum. The 3.1 eV difference between the oxidation and the reduction onsets agree nicely with the 400 nm (3.1 eV) HOMO−LUMO gap, as determined by the onset of PTPD absorption peak depicted in Figure 2. As expected, the CV of the $TMTPD^{\bullet+}$ SbF_6^- radical salt, exhibited a lowering in both the oxidation (0.23 V) and reduction (−2.35 V) peaks as compared to PTPD. The onsets of these oxidation and reduction waves correspond to 5.03 and 2.45 eV with respect to vacuum with a difference of 2.58 eV, which is in agreement with the primary absorption peak (490 nm, 2.53 eV) of the $TMTPD^{\bullet+}$ SbF_6^- radical salt.

Binary PTPD/Salt Devices. Figure 4 illustrates the *J*−*V* characteristics under illumination of the binary PTPD/salt devices as a function of concentration. The corresponding *J*−*V* characteristics under no illumination are shown in Figure S3 of the Supporting Information. The thicknesses of all devices were around 2500 Å. No considerable thickness variation was observed with incorporation of various amounts of the radical salt. All the devices exhibited a distinct photovoltaic effect as evident by the nonzero values of current density and open circuit voltage in the fourth quadrant.

The variation of the open circuit voltage and short circuit current of these devices with increasing salt concentrations in the polymer is shown in Figure 5A. Figure 5B,C illustrates the energy levels of PTPD (within curly brackets) and the radical salt (within square brackets) with respect to the Fermi levels of ITO and Al electrodes. The active region of this device is shaded gray indicating that only the portion adjacent to the Al electrode contributes to photovoltaic current due to limited transport of electrons in the PTPD/salt binary

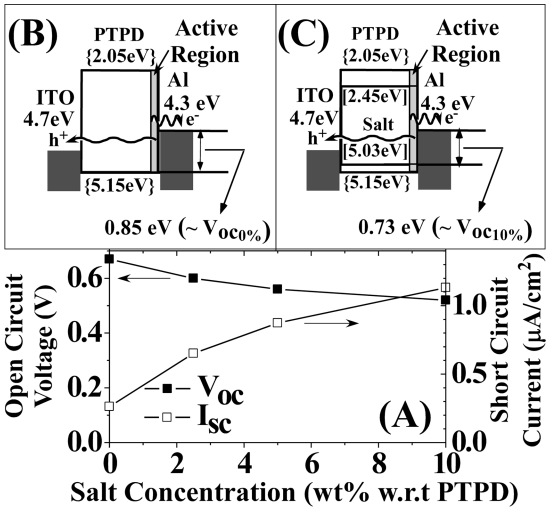

Figure 5. Variation of the short circuit current (open squares, right ordinate) and open circuit voltage (filled squares, left ordinate) of ITO/PTPD−salt/Al binary blend devices for various salt concentrations in the polymer. (A) Energy diagrams for these binary blend devices in the absence (B) and presence (C) of the radical salt.

blend. The short circuit current (I_{sc}) of these binary blend devices increased with increasing salt concentration suggesting the favorable role played by the radical salt. This increase in I_{sc} can be attributed to (i) increase in hole conductivity of the binary blend matrix, which lowers the series resistance for hole transport (evident from the dark *J*−*V* curves shown in Figure S3 of Supporting Information) and (ii) an increase in absorbance due to the addition of the radical salt. The comparison between the percent increase in the absorption of the PTPD/salt films and that of the short circuit density as a function of salt concentration is shown in Figure S5 of the Supporting Information.

The 0% device exhibits a V_{oc} of 0.7 V which upon increasing salt concentration gradually decreases to 0.52 V. Such V_{oc} values are considerably higher than the V_{oc} expected from the metal insulator metal (MIM) model, which for ITO/Al electrode should be of the order of 0.4 V.[33] The gradually decreasing V_{oc} trend can rather be explained by taking into account the pinning of holes to the HOMO of polymer and/or the salt and that of electrons to the Al.[34] If this is the case, the V_{oc} expected for 0% and 10% salt device should be 0.85 and 0.73 V (difference between HOMO of PTPD and salt to that of Al) as shown in Figure 5B,C, respectively. Taking into account the series resistance across these single layer devices, the experimentally observed 0.7 and 0.52 V V_{oc} values for the 0% and 10% salt devices are in close agreement to the theoretically expected 0.85 and 0.73 V values, respectively. In addition, this model can also explain the progressive decrease in V_{oc} for increasing salt concentration as part of the gradual interaction in HOMO values between the PTPD and salt, for various salt concentrations.

As expected the fill factors (FF) and the power conversion efficiencies (η_E) for these binary blend devices are low with the highest FF of 0.3 and highest η_E of 0.012% obtained

(33) Parker, I. D. *J. Appl. Phys.* **1994**, *75*, 1658.
(34) Brabec, C. J.; Cravino, A.; Meissner, D.; Sariciftci, N. S.; Fromherz, T.; Rispens, M. T.; Sanchez, L.; Hummelen, J. C. *Adv. Funct. Mater.* **2001**, *11*, 374.

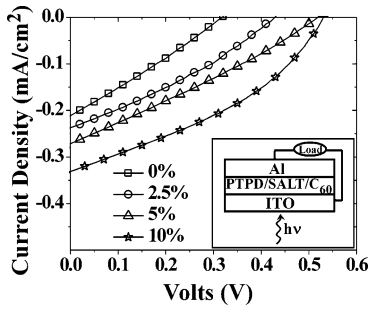

Figure 6. Fourth quadrant $J-V$ characteristics under illumination of the single layer ITO/PTPD−salt−C_{60}/Al ternary blend devices with varying salt concentration. The inset shows the device configuration used.

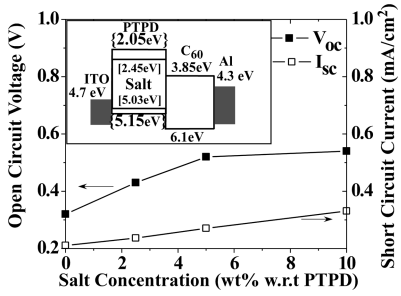

Figure 7. Variation of the short circuit current (open squares, right ordinate) and open circuit voltage (filled squares, left ordinate) of ITO/PTPD−salt−C_{60}/Al ternary blend devices, as a function of salt concentration where the concentration of C_{60} ratio was kept constant at 50 wt % with respect to PTPD. (T1 blend) Inset illustrates the energy levels in these ternary blend devices.

from 10% salt devices. The η_E, though low, increased with increasing salt concentration from 0.00015% for the 0% salt device to 0.012% for the 10% salt device. The low η_E (even for the 10% salt device) can be attributed to the absence of efficient exciton dissociation in these single layer devices, which is mainly localized in the vicinity of the Al electrode. To further boost the exciton dissociation and electron charge transport, the PTPD/salt binary system was blended with an electron acceptor, buckminster fullerene C_{60}. The performance of photovoltaic devices based on these ternary blends of PTPD, salt, and C_{60} were investigated for increasing amount of both salt and C_{60}, designated as T1 and T2, respectively. XRD studies revealed that in these ternary blends, the C_{60} phase crystallizes while the PTPD/salt phase remains amorphous (Figure S2 in Supporting Information). In addition, CV measurements of various mixtures of C_{60} and $TMTPD^{\bullet+}$ SbF_6^- radical salt in various solvents indicated that C_{60} does not form charge-transfer complexes with the radical salt.

Ternary PTPD/Salt/C_{60} Blend Devices. *(a) Variation of Salt.* Figure 6 illustrates the $J-V$ characteristics under illumination of the ITO/T1-blend/Al devices for various salt concentrations (T1 types of devices, with the photoactive layer having C_{60} at a concentration of 50 wt % with respect to PTPD along with the salt which was varied from 0 to 10 wt % with respect to PTPD). $J-V$ characteristics under no illumination are shown in Figure S4 of Supporting Information. Figure 7 shows the variation of short circuit current and open circuit voltage from T1 devices with varying salt concentration. The short circuit current increases with increasing salt concentration, following the same trend as that of binary PTPD/salt devices (Figure 5). In all T1 devices, however, the addition of C_{60} increased the I_{sc} by 2−3 orders of magnitude, which follows the well described behavior of conducting polymers/C_{60} blends suggesting the classical case of photoinduced electron transfer. Such increase of photocarrier generation efficiency is well documented for conjugated polymer/C_{60} devices.[16] This is attributed to the facile exciton dissociation into holes and electrons within the respective polymer and C_{60} phases. As shown in Figure 2, C_{60} also contributes to the absorption of light along with assisting in charge separation and transport of electrons to the cathode. Moreover, C_{60}'s strong tendency to crystallize generates a bulk heterostructure geometry throughout these 2500 Å thick films. The addition of salt increases the I_{sc} from 0.22 mA/cm^2 for the 0% salt device to 0.33 mA/cm^2 for the 10% salt device due to the increase in p-type conductivity of the PTPD phase. In addition to this, as shown in Figure 2, it is expected that the presence of the salt increases the absorption of light by the photoactive film which can also add to the generated photocurrent. This will be the subject of future research.

The V_{oc} in these devices started at 0.34 V for the 0% salt device and increased with increasing salt concentration before saturating at a value of 0.5 V. While reports have indicated that the V_{oc} in acceptor−donor blend devices scales according to the difference of the HOMO of the donor and LUMO of the acceptor, the upper limit of the V_{oc} is limited by the difference in the quasi Fermi levels of the donor and the acceptor.[22,35] It has been reported that the mobility of PTPD[25,36−38] and C_{60}[39] are approximately 10^{-4} and 1 cm^2/(V·s), respectively. Even with an order of magnitude increase in the number of carriers provided by the radical salt, such large mobility imbalance could lead to localization of the "active" region of the device close to the ITO electrode. Moreover, inspite of exciton generation and charge separation, such large imbalance in hole and electron mobility leads to efficient electron extraction rather than hole extraction in the device. This is expected to result in the buildup of an excess density of holes within the device, which shifts the quasi-Fermi level of PTPD upward, thereby lowering the V_{oc} to 0.34 V. The addition of the salt improves hole extraction in the device shifting the quasi Fermi level of the PTPD downward. This results in an increase in the V_{oc} of T1 blend devices with increasing salt concentration as was observed in Figure 7.

(b) Variation of C_{60}. To further verify the origin of V_{oc} in these ternary blend devices the variation of C_{60} concentration was also examined. While the presence of varying amounts of C_{60} might impact heterostructure morphology, the energy levels of PTPD, salt, and C_{60} can to the first approximation explain the origin of V_{oc} in these ternary blend devices. For

(35) Brabec, C. In *Organic Photovoltaics*; Brabec, C., Dyakonov, V., Parisi, J., Sariciftci, N. S., Eds.; Springer-Verlag: Berlin, Germany, 2003.
(36) Antoniadis, H.; Hsieh, B.; Abkowitz, M. A.; Stolka, M. *Appl. Phys. Lett.* **1993**, *62*, 3167.
(37) Jacobs, D. B.; Shen, Y.; Malliaras, G. G. *J. Photochem. Photobiol., A* **2001**, *144*, 53.
(38) Stolka, M.; Yanus, J. F.; Pai, D. M. *J. Phys. Chem.* **1984**, *88*, 4707.
(39) Anthopoulos, T. D.; Singh, B.; Marjanovic, N.; Sariciftci, N. S.; Ramil, A. M.; Sitter, H.; Cölle, M.; Leeuw, D. M. d. *Appl. Phys. Lett.* **2006**, *89*, 213504.

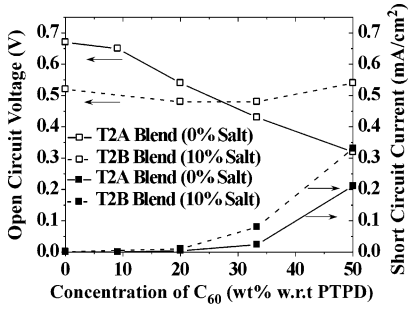

Figure 8. Variation of the short circuit current (open squares, right ordinate) and open circuit voltage (filled squares, left ordinate) of ITO/PTPD−salt−C_{60}/Al devices wherein the concentration of C_{60} in the blend varied from 0 to 50 wt % with respect to PTPD. In the T2A ternary blend devices the salt was fixed at 0 wt % with respect to PTPD, while the T2B ternary blend has a salt concentration of 10 wt % with respect to PTPD.

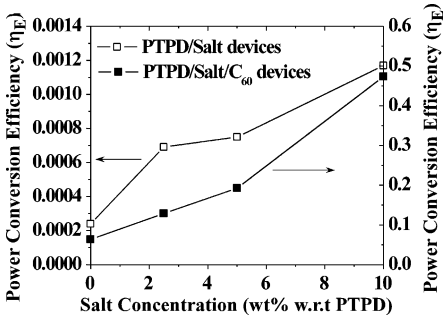

Figure 9. Variation of the power conversion efficiency of ITO/PTPD−salt/Al binary blend (open squares, left ordinate) and ITO/PTPD−salt−C_{60}/Al T1 ternary blend (filled squares, right ordinate) devices wherein the blend has a concentration of C_{60} fixed at 50 wt % with respect to PTPD.

this two sets of ternary blends (T2A and T2B) were prepared. One set (T2A blend) has salt concentration fixed at 0%, and other set (T2B blend) has radical salt concentration of 10% with respect to PTPD polymer. The amount of C_{60} in both sets of T2 devices was varied from 0 to 50% by weight with respect to PTPD. Figure 8 shows the variation of V_{oc} and I_{sc} of both sets of devices. The short circuit current increased with increasing concentration of C_{60} once again confirming the classic case of enhancement of charge generation by using sensitizing agents like C_{60}.[16] The addition of 10% of radical salt further increased I_{sc} by approximately half an order of magnitude

The V_{oc} of the T2A ternary blend (0% salt) devices started at 0.7 V (pure PTPD device) and gradually decreased with increasing C_{60} concentration to a value of 0.34 V. On the basis of the mobility imbalance argument described above, as the concentration of C_{60} increases, it is expected that the "active" region shifts from the Al (see Figure 5B) to the ITO side. Moreover, upon increase in the concentration of C_{60}, the electron extraction becomes increasingly efficient compared to that of hole extraction, leading to a buildup of holes in the device. Such buildup of holes, as described above, shifts the quasi-Fermi level of PTPD upward, which results in a decrease in the V_{oc} with increasing concentration of C_{60}. Upon addition of 10% radical salt, such upward shift of the quasi Fermi level of the PTPD/salt phase is halted as a result of improved hole extraction because of the presence of salt, resulting in a near constant value of observed V_{oc} ($\sim$0.54 V) in these devices. More studies are underway to quantify the origin of V_{oc} in these ternary blend devices as well morphological difference implications on the performance of these ternary blend devices.

Power Conversion Efficiencies of the Binary and Ternary Blend Devices. The variation in the power conversion efficiency of the PTPD/salt/C_{60} ternary T1 devices with increasing salt concentration is shown in Figure 9. The C_{60} remains fixed at 50 wt % in all these devices. For comparison, the variation in the power conversion efficiency of PTPD/salt binary blend devices is also shown. As can be seen, the addition of C_{60} improved the power conversion efficiency by 2−3 orders of magnitude irrespective of amount of salt present. Moreover, similar to the binary PTPD/salt devices, the ternary T1 devices showed an increase in power conversion efficiency with increasing salt concentration, confirming the favorable role of salt in improving the *p*-type conductivity of the PTPD phase.

Conclusions

We have demonstrated that thick (2500 Å) hole-transporting layers doped with radical salts can be used in combination with a photosensitizer (i.e., C_{60}) as an active layer in organic photovoltaic devices. Because of its similar chemical structure to the host polymer, the radical salt helps increase hole conductivity, which in combination with increased absorption increased the I_{sc} of ITO/PTPD−salt/Al devices. The introduction of an electron acceptor C_{60} moiety has led to 2−3 orders of magnitude higher photocurrents. In the "PTPD/salt" binary as well as the "PTPD/salt/C_{60}" ternary blend devices, the power conversion efficiencies increased with increasing salt concentration. Even though the power conversion efficiency for the 10% salt doped ternary ITO/PTPD−salt−C_{60}/Al device was 0.47% (compared to $\sim$5% of the state of the art organic photovoltaic devices),[20] such value is substantial considering that it orginates from a 2500 Å thick amorphous photoactive layer. A more thorough understanding of the influence that processing conditions have on the film morphology, along with optimization of buffer layers on the anode and cathode and dye sensitization of the photoactive layer is expected to further improve device performance and will be reported in future publications. The results presented here, even though specific to the polymer investigated, are expected to be easily extensible to other traditional π-conjugated polymer systems (i.e., polythiophenes) given adequate effort is exerted to properly band-engineer the salt with respect to the host polymer and C_{60}.

Acknowledgment. The authors thank Dr. Bing Hsieh for generously providing the PTPD polymer and the radical salt. The authors acknowledge the help from Jack Gromeck in obtaining the XRD data for the binary and ternary blends. The authors also acknowledge financial support from AFOSR FA9550-06-1-0030, ARO-DAAD-19-02-1-10381, and Department of Defense, U.S. Army Medical Research Grants DAMD17-02-1-0713, W81XWH-04-1-0779, and W81XWH-05-1-0539).

Supporting Information Available: XRD micrographs of the PTPD, the PTPD/salt binary, and PTPD/salt/C_{60} ternary blends are

shown in Figures S1 and S2. $J-V$ characteristics under no illumination of the ITO/PTPD−salt/Al binary blend devices and ITO/PTPD−salt−C_{60}/Al ternary (T1 type) blend devices with varying salt concentration are shown in Figures S3 and S4, respectively. The variation of percent increase in absorption and short circuit current density as a function of radical salt concentration is shown in Figure S5 (PDF). This material is available free of charge via the Internet at http://pubs.acs.org.

CM070744C